J. Min. Metall. Sect. B-Metall. 58 (1) (2022) 129 - 139

Journal of Mining and Metallurgy, Section B: Metallurgy

IMMOBILIZATION OF FLUORIDES FROM SPENT CARBON CATHODE IN A COPPER SMELTING SLAG

L. Li [a, b*], G.-D. Wu [c], F.-G. Tian [a]

[a] College of Environmental Science and Engineering, Donghua University, Shanghai, China
[b] Shanghai Institute of Pollution Control and Ecological Security, Shanghai, China
[c] Faculty of Metallurgical and Energy Engineering, Kunming University of Science and Technology, Kunming, China

(Received 16 June 2021; accepted 03 December 2021)

Abstract

The fluorides from spent carbon cathodes could be effectively solidified in a molten copper smelting slag (FeO-Fe_3O_4-SiO_2-CaO-Al_2O_3) in forms of CaF_2 and $Ca_4Si_2F_2O_7$. The results of thermodynamic analysis, chemical analysis, and XRD and EPMA analyses showed that the F solidification efficiency increased with the CaO amount and decreased with the addition of Al_2O_3 and SiO_2. In addition, it was noteworthy that the F solidification efficiency decreased with an excessive CaO amount, which could be ascribed to the consumption of SiO_2 through forming $CaSiO_3$ and $Ca_3Si_2O_7$. It restricted the solidification of the fluoride into $Ca_4Si_2F_2O_7$. Under the conditions of melting temperature of 1300°C, residence time of 60 min, and N_2 flow rate of 40 ml/min, the optimum CaO and NaF amounts were found to be 20 wt.% and 6 wt.%, respectively, in which the F solidification efficiency in the copper smelting slag of FeO-Fe_3O_4-SiO_2-CaO-Al_2O_3 obtained 98.35%.

Keywords: *Spent carbon cathode; Fluorides; Copper smelting slags; Slag system of FeO-Fe_3O_4-SiO_2-CaO-Al_2O_3; immobilization*

1. Introduction

Spent carbon cathode is a hazardous solid waste that generated from the aluminium electrolysis process, which mainly contains carbon, fluorides (NaF, Na_3AlF_6, and CaF_2 etc.) and other aluminium and cyanide compounds (Al_2O_3, AlN, NaCN, and $Na_3Fe(CN)_6$ etc.) [1-4]. Approximately 10 kg of spent cathode carbon are generated per ton of primary aluminium produced, and approximately 360,000 tons of spent cathode carbon are generated annually in China in recent years [5]. The fluoride and cyanide components in it cause serious soil and water pollution if the spent carbon cathode is landfilled and exposed to air for a long time, and further threaten the growth and health of animals, plants, and humans [6-7]. A harmless treatment of it is urgently needed.

Currently, massive methods for harmless and resource treatment of the spent cathode carbon have been developed, which could be divided into three methods of pyrometallurgical, hydrometallurgical, and pyro and hydro metallurgical corporation processes. The pyrometallurgical process, mainly referring to methods of combustion and vacuum evaporation [8-11] shows advantages on big processing capacity, simple operation, and efficiently detoxification of fluoride and cyanide components. In the combustion process, some calcium compounds (e.g., CaO, $CaCO_3$, and $Ca(OH)_2$) are added to transform and solidify the soluble fluoride into CaF_2, $Ca_4Si_2F_2O_7$ and $Ca_{12}Al_{14}F_2O_{22}$, and meanwhile the cyanide is oxidatively decomposed into N_2 and CO_2 [12-14]. However, the massive consumption of high-quality graphite carbon from the spent cathode carbon makes it difficult to be carried out in an industrial application. In the vacuum evaporation process, the temperature and the vacuum pressure affect the fluoride and cyanide removal rates greatly [10, 11, 15]. The soluble fluoride content could be reduced to 3.5 mg/L and the cyanide was completely decomposed under the conditions of vacuum pressure of 3000 Pa and temperature of 1700°C. However, the huge energy consumption restricts this vacuum evaporation process for an industrial application [15]. Through a hydrometallurgical method the carbon and electrolyte components can be effectively recovered from the spent cathode carbon, and in addition the purity of the obtained carbon exceeds 95% [16-19].

---

[*] *Corresponding author: tianxiametal1008@dhu.edu.cn*

https://doi.org/10.2298/JMMB210616054L

However, massive acid or alkaline wastewater is generated, causing a secondary pollution. The carbon can also be recovered through a combined process of molten salt roasting (Na_2CO_3-Na_2O) and water leaching [20, 21]. The Na_3AlF_6 and CaF_2 were converted to NaF in the molten salt-assisted roasting process, and then could be separated efficiently through the followed water leaching process. Meanwhile, most cyanide was converted into Na_2CO_3, N_2, and CO. As a result, the leachable concentrations of fluoride and cyanide could be decreased to 8.17 mg/L and 0.18 mg/L, respectively, and a graphite carbon with the carbon content of 95.41% was obtained [21]. But the Na_2CO_3 consumption is large, and the soluble fluoride in the leaching water needs a further separation for decreasing a secondary pollution.

To synergistically reutilize the carbon and fluoride components, the spent cathode carbon was used as a reductant in a dilution process of copper converter slags or smelting slags for recovering Cu and/or Co [22-24]. During these processes, the increase of spent cathode carbon both increased the metal recovery and the fluorides solidification efficiency in the final slag [25], and simultaneously the cyanides were transformed to N_2 and CO_2. The leachable F^- and CN^- contents in the final slag were less than 5 mg/L and 0.1 mg/L respectively. It provides a new thought for reusing the spent cathode carbon, but the transformation behaviour of fluorides in the copper slag system was focused little. Based on the thermodynamic analysis, chemical analysis, XRD and EPMA analyses, the transformation of fluorides from the spent carbon cathode in a copper smelting slag of FeO-Fe_3O_4-SiO_2-CaO-Al_2O_3 was researched in this study.

2. Materials and methods

2.1. Materials

2.1.1. Basic slag

Referenced to the chemical and phase compositions of copper smelting slags (Table 1 and Fig.1(a)) obtained from a copper plant located in Yunnan province of China, a basic slag of FeO-Fe_3O_4-SiO_2-CaO-Al_2O_3 was synthesized using pure reagents of FeO, Fe_3O_4, SiO_2, CaO, and Al_2O_3 through a melting process in a N_2 atmosphere. The chemical and phase compositions of this synthesized slag are shown in Table 2 and Fig.1(b), respectively. Figs.1(a) and (b) show that the main phases in the copper smelting slag and synthesized slag are both Fe_2SiO_4 and Fe_3O_4.

2.1.2. Spent cathode carbon

The spent cathode carbon, which was the first cut of the spent pot liner, was obtained from Yunnan Aluminum Co., Ltd of China. The proximate analysis result in Table 3 showing that it contains 73.24wt.% fixed carbon, 25.81wt.% ash, and 0.85wt.% volatile matters. Furthermore, the ash is mainly composed of 9.49wt.% F, 8.44wt.% Na, 3.59wt.% Al_2O_3, and a small amount of CN^- (Table 3). Fig.1(c) identifies the C, NaF, and CaF_2 as the main phases in the spent cathode carbon. Considering the low leachability and little environmental risk of CaF_2 [3], the transformation of NaF was the main focus in this research. The NaF with a purity of 99% was used in this research instead of the spent cathode carbon, and the high-purity nitrogen used with purity of 99.999% was procured from local suppliers.

Table 1. *Chemical composition of the copper smelting slag (wt.%)*

CaO	MgO	Al_2O_3	SiO_2	Fe_3O_4	FeO	others
6.01	3.27	3.49	23.40	1.93	54.82	7.08

Table 2. *Chemical composition of the synthesized basic slag (wt.%)*

Components	FeO	Fe_3O_4	CaO	SiO_2	Al_2O_3	others
Contents	60.52	2.13	6.63	25.83	3.85	1.04

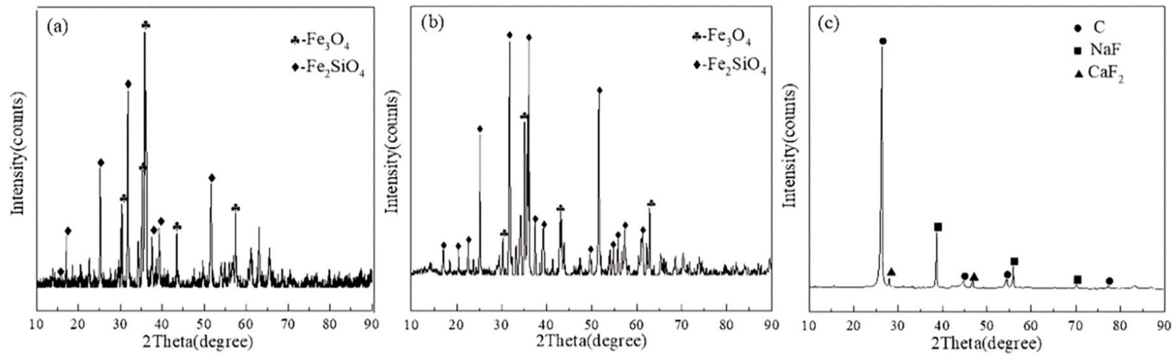

Figure 1. *XRD patterns of the copper smelting slag (a), synthesized basic slag (b) and spent cathode carbon (c)*

Table 3. *Proximate analysis result of the spent cathode carbon and chemical composition of the ash in the spent cathode carbon (wt.%)*

Proximate analysis				Chemical composition of the ash in the spent cathode carbon							
FC_{ad}	M_{ad}	A_d	V_{ad}	F	Na	SiO_2	Al_2O_3	Fe	S	CaO	CN(mg/kg)
73.24	0.10	25.81	0.85	9.49	8.44	1.45	3.59	0.62	0.02	1.86	<0.1

2.2. Methods

The experiments were carried out in a vertical resistance furnace (GSL-1700X-VTQ, Hefei Kejing Materials Technology Co. Ltd., China), and the experimental apparatus is presented in Fig.2. The temperature was precisely measured by a KSY intelligent temperature controller connected to a Pt-Rh thermocouple (accuracy of ±1 °C), which had been corrected by a movable Pt-Rh thermocouple before. For the experimental procedure, the dried synthesized basic slag, NaF and other additives were firstly pre-ground and sieved to below 74 μm, respectively, and then mixed thoroughly at proper mass ratios. After that, the mixture was loaded into a corundum crucible and further placed in the constant-temperature zone of the furnace tube to be heated to 1300 °C in a high-purity N_2 with the flow rate of 40 ml/min. Referenced to a dilution process of copper slags using waste cathode carbon in previous researches [22, 24], the melting temperature, residence time, and N_2 flow rate were controlled at 1300°C, 60 min, and 40 ml/min, respectively, in all the experiments. Then the samples were cooled down to room temperature in the alumina tube under a high-purity N_2 atmosphere with the flow rate of 40 ml/min, pulled out, weighed and ground to prepare for analysis. The F solidification efficiency (SF) in these experiments was calculated using Eq. (I).

$$S_F = \frac{m_2 \times w_2 - m_2 \times w_3}{m_1 \times w_1} \tag{I}$$

where m_1 and m_2 represent the masses of the NaF and final slag, respectively; w_1 and w_2 correspond to the F mass contents in the NaF and final slag (wt. %) respectively, and w_3 corresponds to the leachable F mass content in the final slag (wt. %).

2.3. Characterization

The chemical composition of the sample was analysed using chemical titration and atomic absorption spectroscopy, and the leachable F content in the final slag was detected via an ion chromatography method. All these measurements were conducted three times and the average value was taken as the final result. Phase transformation and microstructure of the sample were detected by X-ray diffraction analysis (XRD, Rigaku, TTR-III) and electron probe microanalysis techniques (EPMA, JXA82, JEOL). For the XRD analysis, the diffraction was measured in 10 to 90 deg 2θ using a Cu Ka radiation at 40kV and 40mA and a step size of 0.01 deg. The thermodynamic analysis was carried out using the FToxid, FTmisc, and FactPS databases in the FactSage 7.2 software.

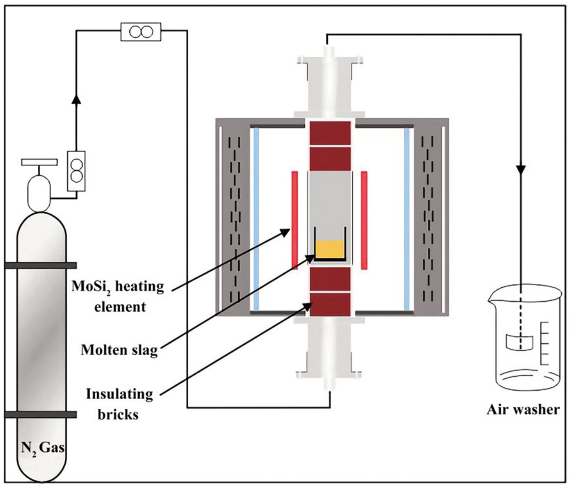

Figure 2. *Schematic diagram of the experimental system*

3. Thermodynamic analysis

To detect the transformation of NaF in the molten synthesized basic slag of FeO-Fe_3O_4-SiO_2-CaO-Al_2O_3, the FactSage 7.2 software was used to calculate equilibrium phases for the reaction system of 100 g synthesized basic slag + 8 g NaF with different addition amounts of CaO, Al_2O_3 and SiO_2 at 1300 °C based on minimizing Gibbs free energy under isothermal, isobaric, and fixed-mass conditions. The results are shown in Fig.3.

With no addition of CaO, Al_2O_3, and SiO_2, Figs.3(a), (b), and (c) show that the NaF was mainly transformed to CaF_2 (s), $NaAlSiO_4$ (l), and $Na_4CaSi_3O_9$ (l) through reactions (1) and (2) when it was melted with the synthesized basic slag. The CaF_2 (s) was then converted into $Ca_4Si_{12}F_2O_7$ (s) through reaction (3) with the CaO addition amount increasing from 0 to 20 wt.% as shown in Fig.3(a). Simultaneously, the Fe_2SiO_4 (l) amount decreases and the FeO (s) amount increases. Increasing the CaO amount further, the amount of $Ca_4Si_2F_2O_7$ (s) decreases while the amounts of NaF (g) and Ca_2SiO_4 (s) increase. The reason might be that massive SiO_2 in the basic slag is combined with CaO forming Ca_2SiO_4 (s) through reaction (4), and then the formation of $Ca_4Si_2F_2O_7$ (s) through reactions (1) and (3) is restricted.

In Fig.3(b), as the SiO_2 addition amount increases from 0 to 15 wt.%, the reaction (5) is promoted, resulting the FeO (s) amount decreases and Fe_2SiO_4 (l) amount increases. Simultaneously, the NaF is mainly transformed to CaF_2 (s). With the SiO_2 addition amount ranging from 10 to 20 wt.%, the $Ca_4Si_2F_2O_7$ (s) is generated through reactions (5) and (3) and increased. Then with more SiO_2 added, the 'F' is transferred from the $Ca_4Si_2F_2O_7$ (s) into the CaF_2 (s), causing the amount of $Ca_4Si_2F_2O_7$ (s) to decrease and that of CaF_2 (s) to increase.

In Fig.3(c), with the increase of Al_2O_3 addition amount from 0 to 4 wt.%, the amounts NaF (g) and Fe_2SiO_4 (l) decrease accompanied by the increase of

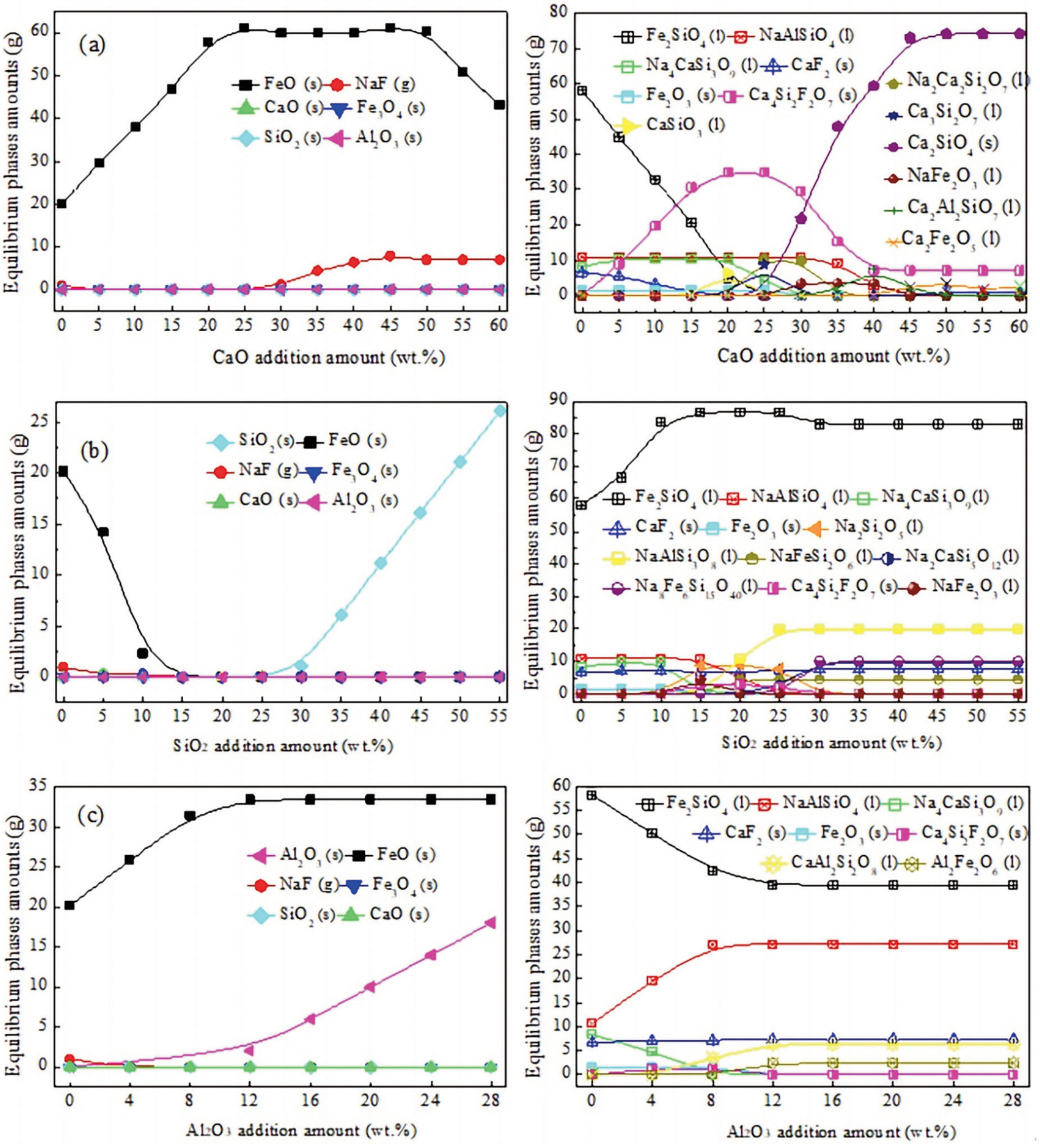

Figure 3. *Effects of CaO, SiO_2 and Al_2O_3 addition amounts on the equilibrium amounts of species in the reaction system of 100 g synthesized basic slag + 8 g NaF at 1300°C*

$NaAlSiO_4$ (l) and FeO (s) amounts, and the ‘F’ in the NaF is mainly transformed to CaF_2 (s) and $Ca_4Si_2F_2O_7$ (s) through reactions (2) and (3). With the Al_2O_3 addition amount exceeding 8 wt.%, more CaO (s) and Fe_2SiO_4 (l) might be reacted with Al_2O_3 (s) forming $CaAl_2Si_2O_8$ (l) and FeO (s) through reaction (6), causing the reaction (3) to be restricted and the $Ca_4Si_2F_2O_7$ (s) amount decreases.

As mentioned above, the ‘F’ in the NaF could be efficiently solidified in the molten slag of FeO-Fe_3O_4-SiO_2-CaO-Al_2O_3 in forms of CaF_2 (s) and/or $Ca_4Si_2F_2O_7$ (s). However, with CaO addition amount over 20 wt.%, the F solidification decreases due to the more formation of Ca_2SiO_4 (s) which restricts the formation of $Ca_4Si_2F_2O_7$ (s).

$$4NaF\ (l)\ +\ 3CaO\ (s)\ +\ 3SiO_2(s)\ =\ 2CaF_2(s)\ +\ Na_4CaSi_3O_9 \tag{1}$$

$$2NaF\ (l)\ +\ Al_2O_3(s)\ +\ 2SiO_2(s)\ +\ CaO\ (s)\ =\ 2NaAlSiO_4(l)\ +\ CaF_2(s) \tag{2}$$

$$3CaO\ (s)\ +\ 2Fe_2SiO_4(l)\ +\ CaF_2(s)\ =\ Ca_4Si_2F_2O_7(s)\ +\ 4FeO\ (s) \tag{3}$$

$$2CaO\ (s)\ +\ SiO_2(s)\ =\ Ca_2SiO_4(s) \tag{4}$$

$$2FeO\ (s)\ +\ SiO_2(s)\ =\ Fe_2SiO_4(l) \tag{5}$$

$$Al_2O_3(s)+\ CaO(s)+\ 2Fe_2SiO_4(l)\ =\ CaAl_2Si_2O_8(l)+\ 4FeO(s) \tag{6}$$

4. Results and discussion

4.1. Effects of CaO addition amount

Based on the thermodynamic analysis above, the effects of CaO addition amount ranging from 0 to 24 wt.% with an interval of 4 wt.% on the F solidification efficiency were firstly assessed under the condition of melting temperature of 1300°C, NaF amount of 10 wt.%, residence time of 60 min, and N_2 flow rate of 40 ml/min.

In Fig. 4(a), the Fe_2SiO_4 diffraction intensity decreases with the CaO amount from 0 to 12 wt.% and disappears at CaO amount of 20 wt.%. Meanwhile, the FeO and $Ca_4Si_2F_2O_7$ appear at CaO addition of 12 wt.% and increase with the CaO amount. Fig. 5 also shows that the Fe and F elements are mainly distributed in the phases of Fe_2SiO_4 and CaF_2, respectively, with no addition of CaO, and the $Ca_4Si_2F_2O_7$ appears at 12 wt.% CaO added. These transformations accord well with the thermodynamic calculation results in Fig. 3(a), indicating that the reactions (1)-(3) could be carried out in the roasting process.

More addition of CaO leads to more formation of CaF_2 and $Ca_4Si_2F_2O_7$ through reactions (1)-(3), as a result of which the F solidification efficiency (S_F) increases with the CaO amount from 0 to 20 wt.% as shown in Fig.4(b). However, increasing the CaO amount further to 24 wt.%, the S_F decreases. It might be due to the consumption of SiO_2 through forming Ca_2SiO_4 by reaction (4) restricts the occurrence of reactions (1)-(3) and some NaF (g) volatilizes into the gas phase as presented in reaction (7) and Fig. 3(a). However, the Ca_2SiO_4 cannot be detected in the final slag according to Fig. 4 (a), the reason for which might be that it transforms to $CaSiO_3$ and $Ca_3Si_2O_7$ during the sample cooling process inferred from Fig. 6 and confirmed by Fig. 4(a). In Fig. 6, during the cooling process of Ca_2SiO_4 from 1300°C to 50 °C, the Ca_2SiO_4 is decomposed and transformed to $CaSiO_3$ (“B” and “D” points), $Ca_3Si_2O_7$ (“B” and “D” points) and CaO (“C” and “E” points). To increase the F solidification efficiency, the CaO addition amount should be controlled at 20 wt.%.

$$NaF(l)\ =\ NaF(g) \tag{7}$$

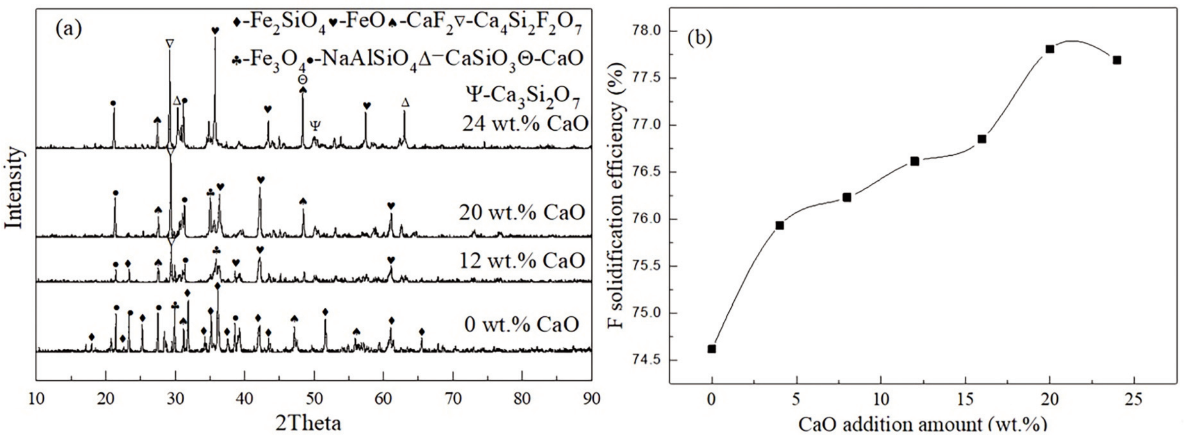

Figure 4. *(a) XRD patterns of the final slag with different CaO addition amounts; (b) Effects of CaO addition amount on the F solidification efficiency in the synthesized basic slag*

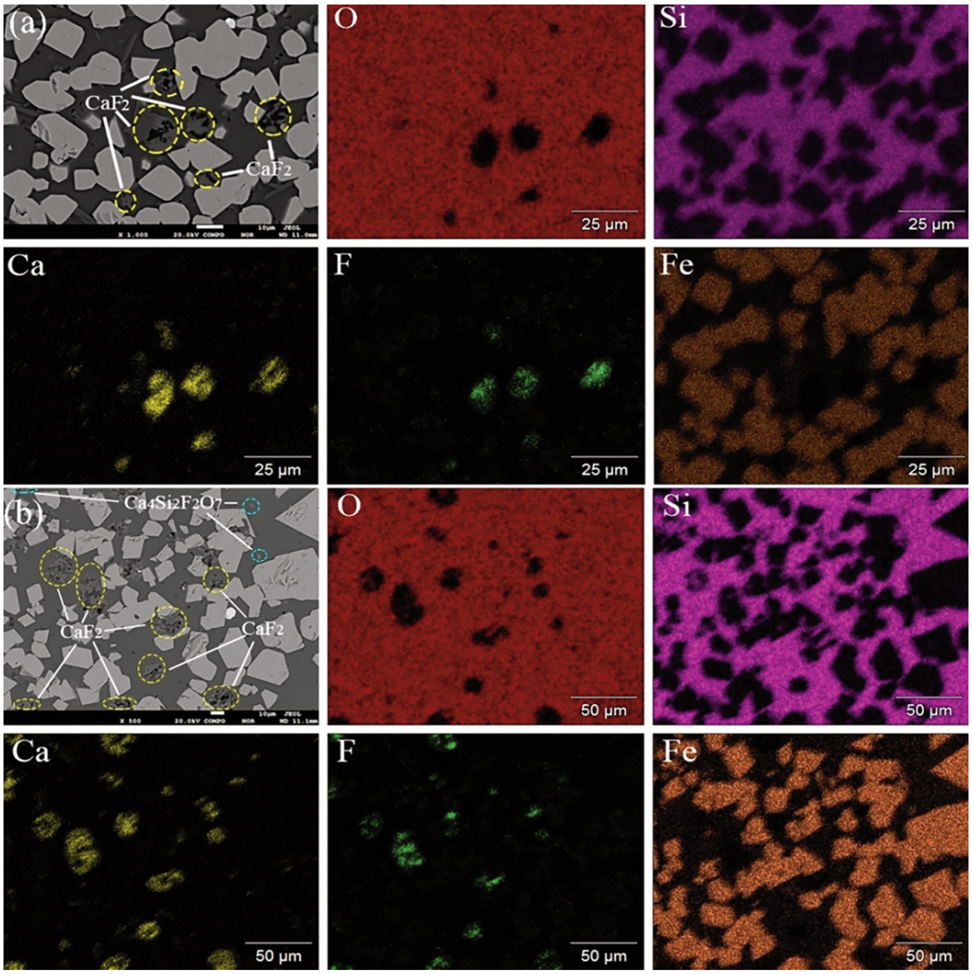

Figure 5. *(a) EPMA mappings of the final slag with no CaO addition; (b) EPMA mappings of the final slag with 12 wt.% CaO added*

4.2. Effects of NaF addition amount

Almost all the F from the NaF could be immobilized in the molten slag of $FeO-Fe_3O_4-SiO_2-CaO-Al_2O_3$ as deduced from Fig. 3, but the F solidification efficiency in Fig. 4(b) is low, around 75%. The equilibrium amounts of species for 100 g synthesized basic slag and 20 g CaO roasted with different NaF amount at 1300 °C were calculated and the results are shown in Fig. 7. Fig. 7 shows that with the NaF amount from 0 to 14 wt.%, almost all the F could be solidified in forms of $Ca_4Si_2F_2O_7$ (s) and CaF_2 (s) thermodynamically. In details, with the increase of NaF amount from 0 to 3 wt.%, the $Ca_4Si_2F_2O_7$ (s), $Ca_3Si_2O_7$ (l) and $NaAlSiO_4$ (l) are formed and increased, accompanied by the decrease of $Ca_2Al_2SiO_7$ (l) and $CaSiO_3$ (l), which might be due to the occurrence of reaction (8). Increasing the NaF amount over 9 wt.%, some $Ca_4Si_2F_2O_7$ (s) can be transformed to CaF_2 (s) through reaction (9), causing the amounts of $Ca_4Si_2F_2O_7$ (s) and Fe_2SiO_4 (l) to decrease and that of $Na_4CaSi_3O_9$ (l), CaF_2 (s) and FeO (s) to increase. The EPMA results in Fig.8 accord well with this F transformation, in which the $Ca_4Si_2F_2O_7$ amount decreases and CaF_2 amount increases with the

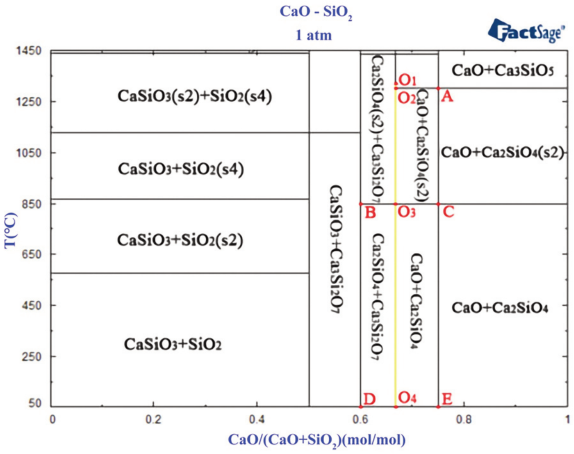

Figure 6. *Phase diagram of CaO-SiO$_2$ at different temperatures*

NaF amount from 8 to 10 wt.%. While the NaF amount increases over 14 wt.%, except for the solidification by the synthesized basic slag, some NaF can evaporate into the gas phase through reaction (7).

The effect of NaF amount ranging from 2 to 12 wt.% on the F solidification efficiency was then experimentally researched under the conditions of melting temperature of 1300°C, CaO addition amount of 20 wt.%, residence time of 60 min, and N_2 flow rate of 40 ml/min; the results are shown in Fig.9. The increase of NaF amount promotes the formation of $Ca_4Si_2F_2O_7$ and CaF_2 through reactions (1)-(3), (8), and (9), as a result of which their intensities in the XRD analysis results increase with NaF amount as

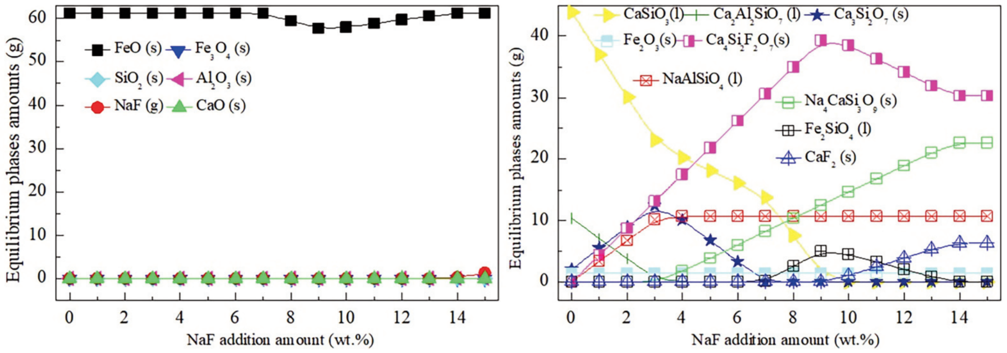

Figure 7. *Effects of NaF amount on the equilibrium amounts of species in the reaction system of 100 g synthesized basic slag + 20 g CaO at 1300°C*

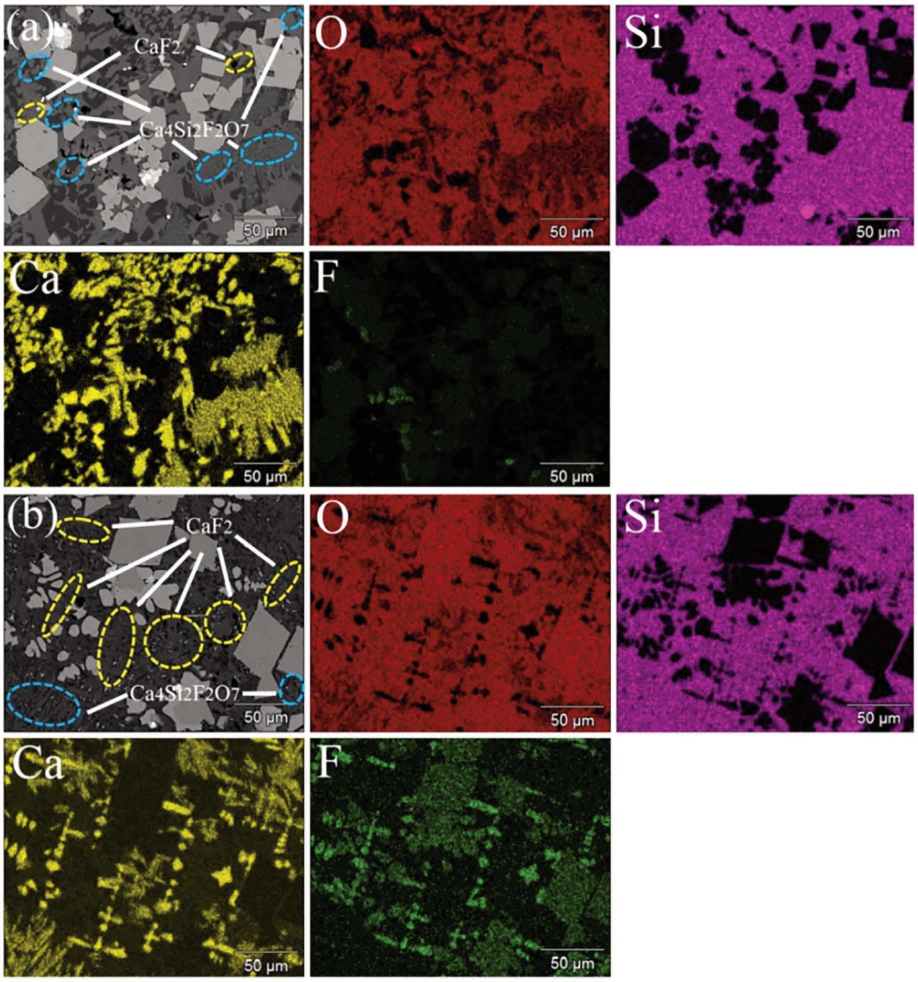

Figure 8. *(a) EPMA mappings of the final slag with 20 wt.% CaO and 8 wt.% NaF addition; (b) EPMA mappings of the final slag with 20 wt.% CaO and 10 wt.% NaF addition*

shown in Fig.9(a). However, the F solidification efficiency (S_F) decreases greatly from 98.35% to 56.90% with the NaF amount from 6 to 12 wt.% as shown in Fig. 9(b), which is not consistent with the thermodynamic results in Fig.7. The reason might be that some NaF had been evaporated into the gas phase before the solidification, which could be confirmed by the more formation of gas pores in the final slag at a more NaF addition as shown in Fig.10. To decrease the environmental pollution caused by the F evaporation, the NaF amount should not be higher than 6 wt.%.

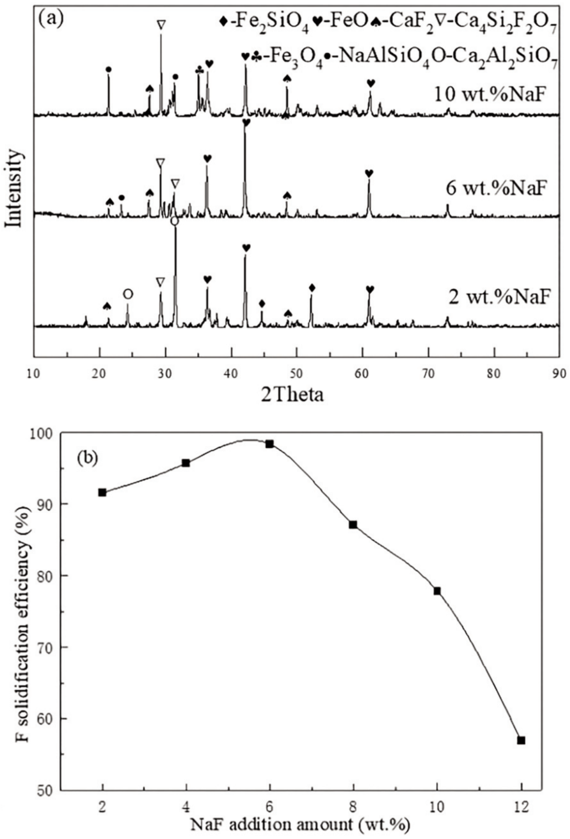

Figure 9. *(a) XRD patterns of the final slag with different NaF amount; (b) Effects of NaF amount on the F solidification efficiency in the synthesized basic slag*

$$Ca_2Al_2SiO_7(l) + 5CaSiO_3(l) + 2NaF\ (l) = Ca_4Si_2F_2O_7(s) + Ca_3Si_2O_7(l) + 2NaAlSiO_4(l) \quad (8)$$

$$Ca_4Si_2F_2O_7(s) + 4NaF\ (l) + Fe_2SiO_4(l) = 3CaF_2(s) + Na_4CaSi_3O_9(l) + 2FeO\ (s) \quad (9)$$

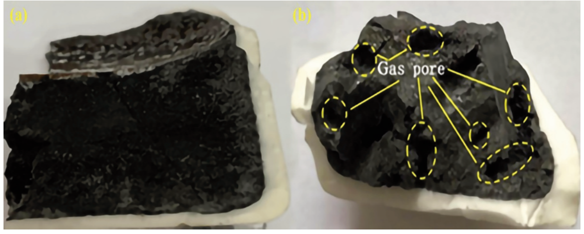

Figure 10. *Apparent morphology of the final slag with NaF amount of 6 wt.% and 10 wt.% respectively*

4.3. Effects of Al_2O_3 and SiO_2 addition amounts

In the conditions of melting temperature of 1300°C, residence time of 60 min, N_2 flow rate of 40 ml/min, CaO and NaF addition amounts of 20 wt.% and 6 wt.%, respectively, the changes of F solidification efficiency with Al_2O_3 and SiO_2 amounts are shown in Fig.11(a) and (b), respectively.

Fig. 11(a) shows that the F solidification efficiency decreases greatly with the increase of Al_2O_3 addition amount, which differs greatly with the thermodynamic calculation results in Fig. 3(b). The reason might be that some CaO are consumed through forming $Ca_2Al_2SiO_7$ (Fig. 12(a)), and the solidification of F through forming CaF_2 and $Ca_4Si_2F_2O_7$ is restricted, deduced from reactions (1)-(3). In Fig.12(a), compared to the phase composition of the final slag without extra Al_2O_3 addition, the $Ca_2Al_2SiO_7$ could be found at a Al_2O_3 addition of 8 wt.% and increases with the Al_2O_3 amount increased

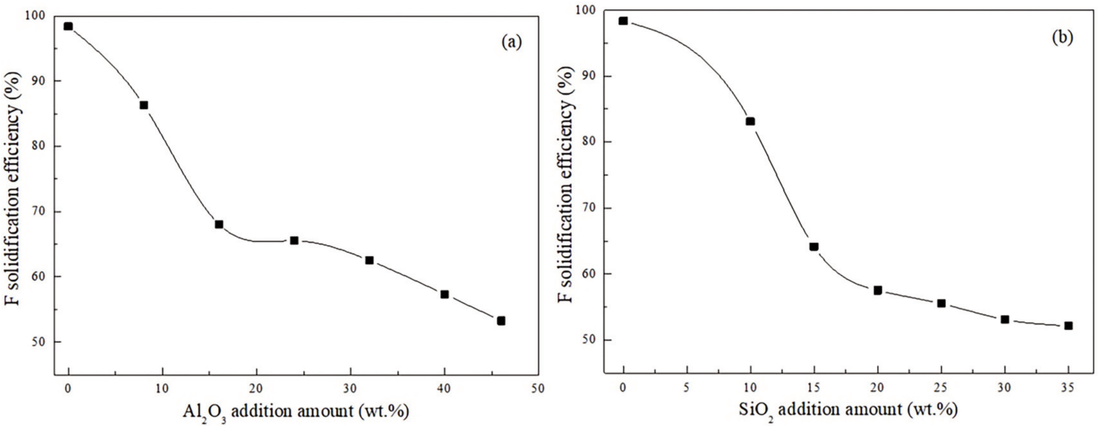

Figure 11. *Effects of Al_2O_3 (a) and SiO_2 (b) addition amounts on the F solidification efficiency in the synthesized basic slag*

to 20 wt.%. Also due to the consumption of CaO by adding SiO_2 through forming $Ca_2Al_2SiO_7$ and $CaSiO_3$ (Fig. 12(b)), the F solidification efficiency decreases obviously with the SiO_2 addition as shown in Fig. 11(b). Fig. 12(b) shows that the $Ca_2Al_2SiO_7$ and $CaSiO_3$ can be generated at a SiO_2 amount of 10 wt.% and increase with the SiO_2 addition amount. To increase the F solidification efficiency in the synthesized basic slag, the extra Al_2O_3 and SiO_2 should not be added.

Moreover, the value of leachable F^- in the final slag was detected via ion chromatography method and found to be 3.67 mg/L, which is far less than the national allowable emission concentration in China as shown in Table 4. It implies that the final slag might be treated as a general solid waste.

Table 4. *Detection of leaching toxicity of the final slag*

Sample	Final slag	National allowable emission concentration in China	Analytical approach
F ($mg\cdot L^{-1}$)	3.67	<100	Ion chromatography

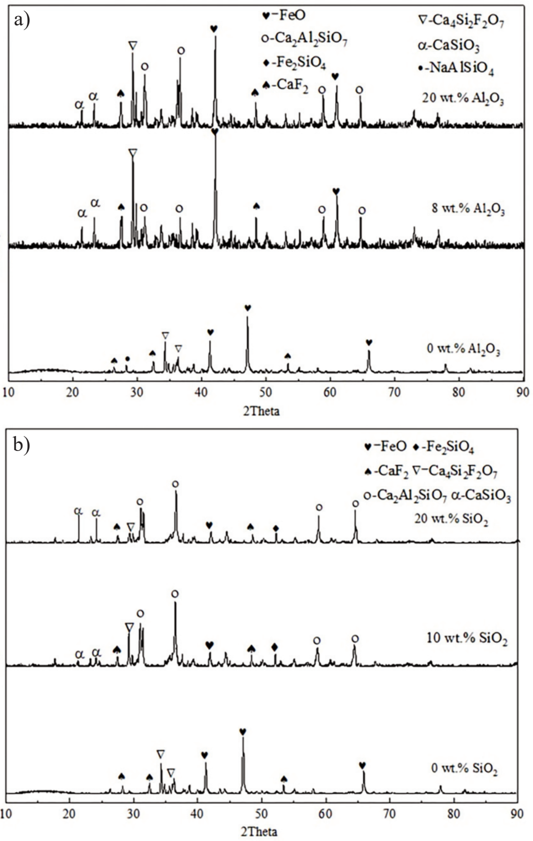

Figure 12. *(a) XRD patterns of the final slag with Al_2O_3 addition amount of 0 wt.%, 8 wt.% and 20 wt% respectively; (b) XRD patterns of the final slag with SiO_2 addition amount of 0 wt.%, 10 wt% and 20 wt.% respectively*

5. Conclusions

The results showed that the NaF could be effectively solidified in the molten slag of FeO-Fe_3O_4-SiO_2-CaO-Al_2O_3.

The 'F' from NaF was mainly transformed to CaF_2 and $Ca_4Si_2F_2O_7$ in the slag of FeO-Fe_3O_4-SiO_2-CaO-Al_2O_3. In a certain range, more addition of CaO led to more formation of CaF_2 and $Ca_4Si_2F_2O_7$, and the F solidification efficiency increased with it. However, with the CaO addition amount exceeding 20 wt.%, some SiO_2 in the synthesized basic slag would be consumed by forming $CaSiO_3$ and $Ca_3Si_2O_7$, which restricted the solidification of NaF into $Ca_4Si_2F_2O_7$. It caused some NaF volatilized into the gas phase and the F solidification efficiency decreased. Similarly, the addition of Al_2O_3 and SiO_2 also hindered the formation of CaF_2 and $Ca_4Si_2F_2O_7$ and decreased the F solidification efficiency through their priority combination with CaO forming $Ca_2Al_2SiO_7$ and/or $CaSiO_3$. Under the conditions of melting temperature of 1300°C, residence time of 60 min, and N_2 flow rate of 40 ml/min, the optimum CaO and NaF amounts were found to be 20 wt.% and 6 wt.%, respectively, in which the F solidification efficiency in the copper smelting slag of FeO-Fe_3O_4-SiO_2-CaO-Al_2O_3 obtained 98.35%.

Acknowledgments

The authors wish to express thanks to the Fundamental Research Funds for the Central Universities, DHU Distinguished Young Professor Program (LZB2021003) and the National Natural Science Foundation of China (51874153) for the financial support of this research.

Author's contributions

Lei LI performed the data analyses and wrote the manuscript, Guo-dong WU performed the analysis with constructive discussions, Feng-guo TIAN contributed to the validation of this study.

Conflict of interest

Lei LI, Guo-dong WU and Feng-guo Tian declare that they have no conflict of interest.

References

[1] L. F. Andrade-vieira, L. C. Davide, L. S. Gedraite, J. M. S. Campos, H. Azevedo, Genotoxicity of SPL (spent pot lining) as measured by Tradescantia bioassays, Ecotoxicology and Environmental Safety, 74 (2011) 2065-2069. https://doi.org/10.1016/j.ecoenv.2011.07.008.

[2] T. K. Pong, R. J. Adrien, J. Besida, T. A. O'donnell, D.

G. Wood, Spent potling – A hazardous waste made safe, Process Safety and Environmental Protection, 78 (2000)204-208. https://doi.org/10.1205/095758200530646.

[3] K. Yang, Z. L. Tao, K. P. Wang, Z. L. Tian, Y. Q. Lai, Upcycling of spent carbon cathode (SCC) into SCC-2600@rGO facilitates ultrastable and fast lithium storage, Journal of Alloys and Compounds, 877 (2021) 160196. https://doi.org/10.1016/j.jallcom.2021.160196.

[4] D. F. Lisbona, C. Somerfield, K. M. Steel, Leaching of spent pot-lining with aluminum anodizing wastewaters: Fluoride extraction and thermodynamic modeling of aqueous speciation, Industrial & Engineering Chemistry Research, 51(2012) 8366-8377. https://doi.org/10.1021/ie3006353.

[5] D. F. Lisbona, C. Somerfield, K. M. Steel, Leaching of spent pot-lining with aluminium nitrate and nitric acid: Effect of reaction conditions and thermodynamic modelling of solution speciation, Hydrometallurgy, 134-135 (2013) 132-143. https://doi.org/10.1016/j.hydromet.2013.02.011.

[6] Y. Y. Wang, Y. J. Luo, H. Xu, H. J. Xiao, Corrosion behavior and electrochemical property of Q235A steel in treated water containing halide ions (F-, Cl-) from nonferrous industry, Journal of Central South University, 27 (2020) 1224−1234. https://doi.org/10.1007/s11771-020-4362-6

[7] K. W. Dong, F. Xie, W. Wang, Y. F. Chang, D. K. Lu, X. W. Gu, C. L. Chen, The detoxification and utilization of cyanide tailings: A critical review, Journal of Cleaner Production, 302 (2021) 126946. https://doi.org/10.1016/j.jclepro.2021.126946

[8] G. Holywell, R. Breault, An overview of useful methods to treat, recover, or recycle spent potlining, Journal of Metals, 65 (2013) 1441-1451. https://doi.org/10.1007/s11837-013-0769-y.

[9] M. Y. Luo, X. P. Gu, T. Qu, L. Shi, Y. N. Dai, F. Lv, Y. Tian, Separation of electrolyte and carbon from electrolytic aluminum spent cathode carbon block by vacuum distillation, Nonferrous Metals Engineering, 10 (2020) 47-52 (in Chinese). https://doi.org/10.3969/j.issn.2095-1744.2020.07.008.

[10] Y. W. Wang, J. P. Peng, Y. Z. Di, Separation and recycling of spent carbon cathode blocks in the aluminum industry by the vacuum distillation process, Journal of Metals, 70 (2018) 1877-1882. https://doi.org/10.1007/s11837-018-2858-4.

[11] K. Yang, Z. J. Zhao, X. Xin, Z. L. Tian, K. Peng, Y. Q. Lai, Graphitic carbon materials extracted from spent carbon cathode of aluminium reduction cell as anodes for lithium ion batteries: Converting the hazardous wastes into value-added materials, Journal of the Taiwan Institute of Chemical Engineers, 104 (2019) 201-209. https://doi.org/10.1016/j.jtice.2019.09.012.

[12] W. M. Xie, F. P. Zhou, J. Y. Liu, X. L. Bi, Z. J. Huang, Y. H. Li, D. D. Chen, H. Y. Zou, S. Y. Sun, Synergistic reutilization of red mud and spent pot lining for recovering valuable components and stabilizing harmful element, Journal of Cleaner Production, 243 (2020) 118624. https://doi.org/10.1016/j.jclepro.2019.118624.

[13] X. L. Wang, X. C. Chen, Development status of processing technology for spent potlining in China, Essential Readings in Light Metals, (2016) 1064-1066. https://doi.org/10.1007/978-3-319-48200-2_143.

[14] G. Sun, G. Zhang, J. Y. Liu, W. M. Xie, F. Evrendilek, M. Buyukada, (Co-)combustion behaviors and products of spent potlining and textile dyeing sludge, Journal of Cleaner Production, 224 (2019) 384-395. https://doi.org/10.1016/j.jclepro.2019.03.208.

[15] M. Z. Xie, R. B. Li, H. L. Zhao, W. Liu, T. T. Lu, F. Q. Liu, Detoxification of spent cathode carbon blocks from aluminum smelters by joint controlling temperature-vacuum process, Journal of Cleaner Production, 249 (2020) 119370. https://doi.org/10.1016/j.jclepro.2019.119370.

[16] K. Yang, P. Y. Gong, Z. L. Tian, K. Peng, Y. Q. Lai, Carbon recovered from spent carbon cathode of aluminum reduction cell towards its valorisation as negative electrodes for lithium ion batteries, Diamond and Related Materials, 109 (2020) 108062. https://doi.org/10.1016/j.diamond.2020.108062.

[17] J. Xiao, J. Yuan, Z. L. Tian, K. Yang, Z. Yao, B. L. Yu, L. Y. Zhang, Comparison of ultrasound-assisted and traditional caustic leaching of spent cathode carbon (SCC) from aluminum electrolysis, Ultrasonics Sonochemistry, 40 (2018) 21-29. https://doi.org/10.1016/j.ultsonch.2017.06.024.

[18] J. Yuan, J. Xiao, F. C. Li, B. J. Wang, Z. Yao, B. L. Yu, L. Y. Zhang, Co-treatment of spent cathode carbon in caustic and acid leaching process under ultrasonic assisted for preparation of SiC, Ultrasonics Sonochemistry, 41 (2018) 608-618. https://doi.org/10.1016/j.ultsonch.2017.10.027.

[19] Z. N. Shi, W. Li, X. W. Hu, B. J. Ren, B. L. Gao, Z. W. Wang, Recovery of carbon and cryolite from spent pot lining of aluminium reduction cells by chemical leaching, Transactions of Nonferrous Metals Society of China, 22 (2012) 222-227. https://doi.org/10.1016/S1003-6326(11)61164-3.

[20] Z. Yao, Q. F. Zhong, J. Xiao, S. C. Ye, L. Tang, Z. A. Wang, Efficient separation of fluoride and graphite carbon in spent cathode carbon from aluminum electrolysis by mechanical activation assisted alkali fusion treatment, Minerals Engineering, 161 (2021) 106717. https://doi.org/10.1016/j.mineng.2020.106717

[21] Z. Yao, Q. F. Zhong, J. Xiao, S. C. Ye, L. Tang, Z. H. Zhang, An environmental-friendly process for dissociating toxic substances and recovering valuable components from spent carbon cathode, Journal of Hazardous Materials, 404 (2021) 124120. https://doi.org/10.1016/j.jhazmat.2020.124120

[22] K. X. Mao, L. Li, Reduction and dilution of converter copper slag with spent cathode carbon in aluminum electrolysis, Nonferrous Metals Engineering, 10 (2020) 65-72. (in Chinese). https://doi.org/10.3969/j.issn.2095-1744.2020.10.011.

[23] S. Hong, W. Liu, F. Q. Liu, Preliminary study on reduction and extraction of copper and cobalt from copper converter slag by using waste cathode carbon block, Light Metals, 8 (2019) 41-45. (in Chinese). https://doi.org/10.13662 /j.cnki.qjs.2019.08.009.

[24] G. D. Wu, L. Li, K. Z. Li, Y. Yu, Dilution of Isa copper smelting slag by carbothermic reduction with waste cathode carbon, The Chinese Journal of Process Engineering, 10 (2021) 1-9. (in Chinese). https://doi.org/10.12034/j.issn.1009-606X.220327

[25] K. X. Mao, L. Li, M. Xu, Iron and copper recovery from copper slags through smelting with waste cathode carbon from aluminium electrolysis, Journal of Central South University, 28 (2021) 2010−2021. https://doi.org/10.1007/s11771-021-4749-z.

IMOBILIZACIJA FLUORIDA IZ POTROŠENE UGLJENIČNE KATODE U ŠLJACI IZ POSTUPKA DOBIJANJA BAKRA

L. Li [a, b*], G.-D. Wu [c], F.-G. Tian [a]

[a] Fakultet za nauku o zaštiti okoline i inženjerstvo, Donghua Univerzitet, Šangaj, Kina
[b] Šangajski institut za kontrolu zagađenja i ekološku sigurnost, Šangaj, Kina
[c] Fakultet za metalurško i energetsko inženjerstvo, Univerzitet nauke i tehnologije u Kunmingu, Kunming, Kina

Apstrakt

Fluoridi iz potrošenih ugljeničnih katoda mogu biti efikasno solidifikovani u rastopljenoj šljaci iz postupka dobijanja bakra (FeO-Fe_3O_4-SiO_2-CaO-Al_2O_3) u obliku CaF_2 i $Ca_4Si_2F_2O_7$. Rezultati termodinamičkih, hemijskih, kao i XRD i EPMA analiza pokazali su da je efikasnost solidifikacije F rasla sa količinom CaO, i smanjivala se dodavanjem Al_2O_3 i SiO_2. Uz to, značajno je to što je efikasnost solidifikacije F opadala sa velikom količinom CaO, što se može pripisati potrošnjom SiO2 kroz formiranje $CaSiO_3$ i $Ca_3Si_2O_7$. Ovo je ograničavalo solidifikaciju fluorida u $Ca_4Si_2F_2O_7$. Pod uslovima temperature topljenja od 1300°C, trajanja od 60 min, protoku N_2 od 40 ml/min, pronađeno je da su optimalne količine CaO i NaF 20 wt.% i 6 wt.%, pojedinačno, gde je efikasnost solidifikacije F u bakrenoj šljaci FeO-Fe_3O_4-SiO_2-CaO-Al_2O_3 dostigla 98.35%.

Ključne reči: *Potrošena karbonska katoda; Fluoridi; Bakrena šljaka; Sistem šljake FeO-Fe_3O_4-SiO_2-CaO-Al_2O_3; imobilizacija*